Improving curving performance of a straddle type monorail vehicle by using semi-active devices

Ali S. Yıldız*

Department of Mechanical Engineering,
Sivas University of Science and Technology,
Sivas, Turkey
Email: suat@sivas.edu.tr
*Corresponding author

S. Sivrioğlu

Department of Mechanical Engineering,
Antalya Bilim University,
Antalya, Turkey
Email: selim.sivrioglu@antalya.edu.tr

Abstract: This paper is concerned with improving the curving performance of the monorail vehicles which are one of the modern mass transport systems, by using semi-active magnetorheological (MR) dampers. Controlling the curving dynamic of the monorail vehicles with semi-active devices is a new research area. The considered monorail vehicle has one segment supported by two bogies. As a secondary suspension, lateral and vertical MR dampers are taken into consideration in addition to air suspensions. Control performances of the robust H_∞ and adaptive control are investigated and compared with passive case along a designed road profile. Parametric uncertainties in running tyres and vehicle mass are taking into consideration in the control simulations. Simulation results show that the designed controllers improved the roll, yaw and vertical motions of the monorail vehicle when compared to uncontrolled and passive cases. These improvements provide better comfort and safer condition as well as small turning radius can be achieved by monorail vehicles equipped with the semi-active suspension system.

Keywords: semi-active suspension; MR damper; adaptive controller; monorail vehicle; H_∞ control.

Reference to this paper should be made as follows: Yıldız, A.S. and Sivrioğlu, S. (2021) 'Improving curving performance of a straddle type monorail vehicle by using semi-active devices', *Int. J. Heavy Vehicle Systems*, Vol. 28, No. 3, pp.385–408.

Biographical notes: Ali S. Yıldız received his Bachelor's degree in Mechanical Engineering from the Celal Bayar University in 2008. He received his MSc in Mechanical Engineering from the Gebze Institute of Technology in 2013. He is currently a Research Assistant and a PhD student at Gebze Technical University. His research interests include nonlinear control applications, superconductive levitation, dynamic system modelling and control, and magnetorheological dampers.

S. Sivrioğlu received his PhD from Chiba University, Chiba, Japan, in 1998. He is currently a Professor in the Department of Mechanical Engineering, Gebze Technical University, Gebze, Turkey. His current research interests are modelling and experimental verification of superconducting magnetic levitation, active control of magnetic bearings, semi-active control of vehicle suspension systems, robust and adaptive control applications.

1 Introduction

The straddle-type monorail vehicles have certain differences from traditional rail vehicles. This system has a separate right of way, which has no influence on the current ground transportation system (Bao et al., 2016). They stride over the guideway and run above it. Monorail vehicles have three types of tyres such as running, guide and stabilisation tyres. While running tyres provide the longitudinal movement, guide tyres lead the truck along the guideway. In addition, stabilisation tyres prevent excessive rolling motion of the vehicle. Monorail transit systems have some advantages such as low manufacturing cost comparing subway systems, low running noise and good climbing ability. They can also be operated driverless on the small radius of curve tracks (Kato et al., 2004; Goda et al., 1999).

In literature, there are few researches on the dynamic behaviour of the monorail systems under the different segment of the guideway, particularly on the suspension control units. Maciel and Barbosa (2016) considered the three degrees of freedom monorail vehicle. They studied the combination of linear and nonlinear cornering stiffness and slip velocities to calculate tyre forces at contact points under the misalignment of the guideway inputs. A dynamic simulating software of 18 degrees of freedom monorail vehicle was developed by Wang et al. (2017) to investigate the effect of the curve radius, driving speed and vehicle load on the dynamic response of the straddle monorail track beam. Results show that displacements in vertical and lateral direction is directly proportional to vehicle speed and load. Du et al. (2014) showed that straddle-type monorail vehicle driving safety deterioration arises with the failing of the air springs by considering six failure conditions. Also, guide tyres appear derailment phenomenon that affects the safety of the vehicle.

In monorail vehicles, severe uneven wear of the running wheel will also lead to the significant reduction of the adhesion ability of the running wheel (Wen et al., 2016; Du et al., 2017). In this study, tyre dynamics are not considered instead of that all tyres are modelled as linear springs and dashpots taking into considerations parametric uncertainties that corresponding to tyre wear. Also, monorail vehicle weight is a variable parameter with respect to number of passengers, therefore, vehicle weight is assumed 15% of its nominal value in suspension control design. In railway system, semi-active components with proper control design have been used for improving performance and stability of an uncertain system (Yıldız et al., 2015; Orvnäs et al., 2011; Zong et al., 2013). However, controlling the translation and rotational dynamics of the monorail vehicle with semi-active devices is a new research area. In this study, straight, transition and circular stages of a track were designed, and a full turn of a monorail vehicle was simulated under parametric uncertainties.

2 Modelling of the monorail vehicle

Straddle type monorail vehicle runs on rubber tyres that straddle a single concrete guideway beam and it has three types of tyres as illustrated in Figure 1 (Hitachi Monorail Technology Presentation, 2013). The running tyres are the main component of the bogie and provide longitudinal motion. Due to the vertical load, most of the wear occurs on the running tyre. Guide tyres at the four corners of the bogie and stabilising tyres at the two side of the bogie, lead the car body along the guideway (Goda et al., 2000). Also, stabilisation tyres prevent excessive rolling motion of the vehicle.

Figure 1 Illustration of the straddle type monorail vehicle (Hitachi Monorail Technology Presentation, 2013) (see online version for colours)

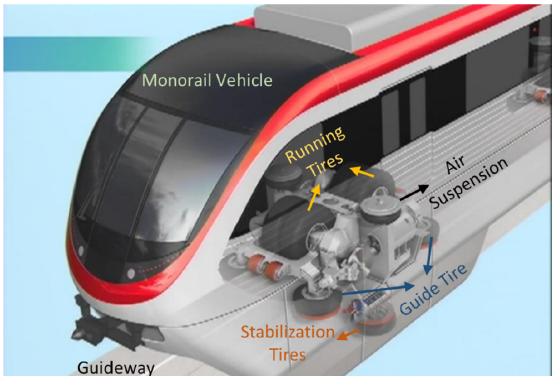

In this study, a 15 degree-of-freedom (DOF) train model is constituted as shown in Figure 2. In the modelling structure, vertical, lateral and rotational dynamics of the monorail vehicle are considered, and the longitudinal dynamics is neglected. It is assumed that the monorail vehicle body and bogies are rigid and the centres of the masses have the coordinate systems $O_c y_c z_c$, $O_{bf} y_{bf} z_{bf}$ and $O_{br} y_{br} z_{br}$, respectively. The DOF variables of the car body and bogies are presented in Table 1. The parameters and their description used in the simulation are stated in Appendix A.

Vertical and lateral air suspensions, installed between the vehicle body and the bogies, are modelled as linear springs and dampers. The bogie frame of the monorail vehicle is connected to the guideway with the running, guide and stabilising tyres. These tyres are modelled as stiffness and damping elements. It is assumed that tyres and guideway maintain constant contact. To apply a semi-active control for suppressing the lateral and rolling movement, a set of MR dampers are positioned next to air suspensions.

Table 1 DOF of the vehicle index

DOF	*Vertical movement*	*Lateral movement*	*Yaw*	*Pitch*	*Roll*
Vehicle body	z_{11}	y_{11}	θ_{z11}	θ_{y11}	θ_{x11}
Front Bogie	z_{21}	y_{21}	θ_{z21}	θ_{y21}	θ_{x21}
Rear Bogie	z_{22}	y_{22}	θ_{z22}	θ_{y22}	θ_{x22}

Figure 2 Schematic view of the idealised monorail vehicle: (a) front view and (b) side and top view (see online version for colours)

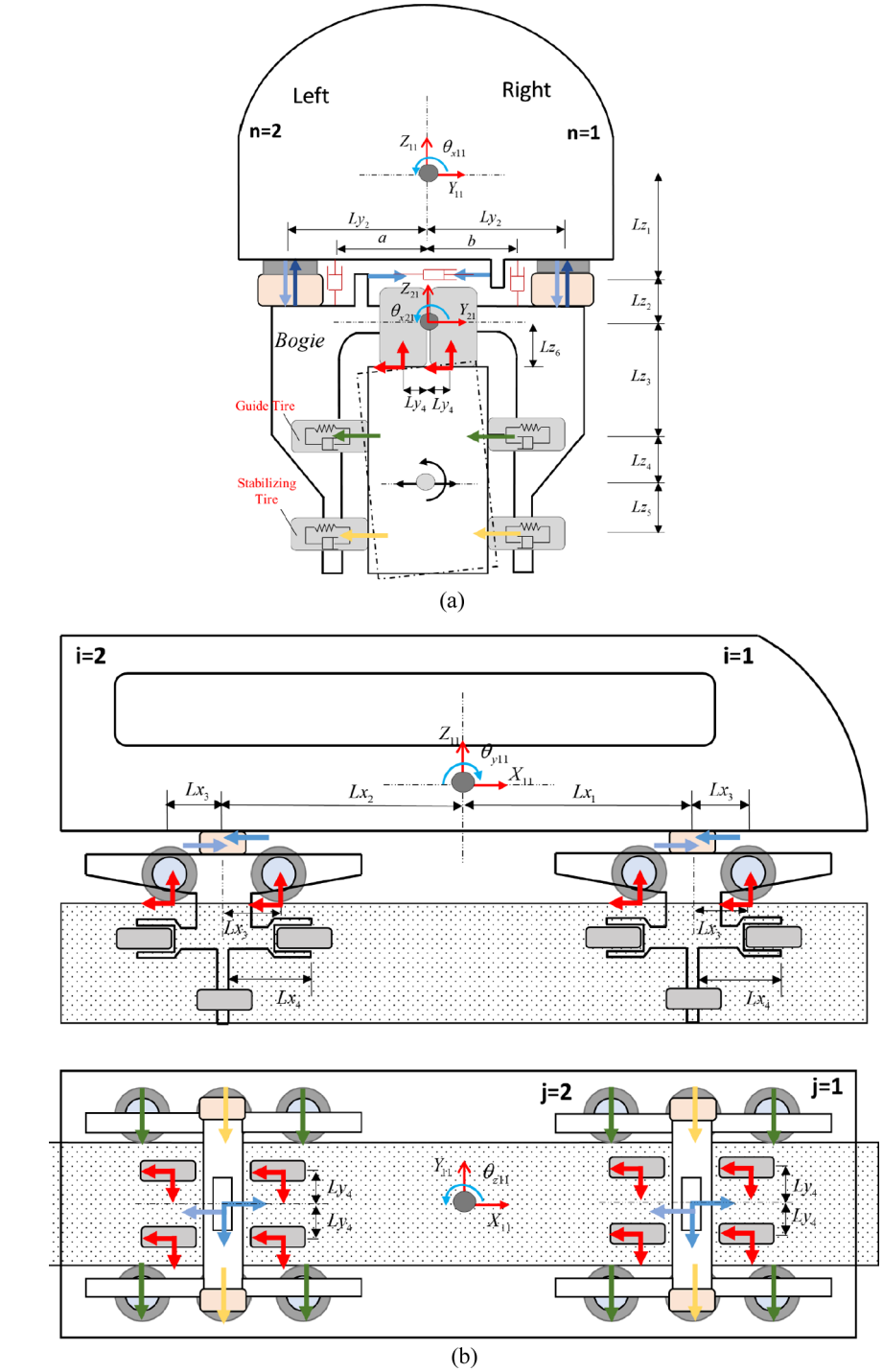

The equations governing the motion of monorail vehicle body and bogies are obtained by using the Lagrange equation of motion, as shown in equation (1).

$$\frac{\mathrm{d}}{\mathrm{d}t}\left(\frac{\partial L}{\partial \dot{q}_i}\right)-\frac{\partial L}{\partial q_i}+\frac{\partial D_E}{\partial \dot{q}_i}=Q_i, \tag{1}$$

where q_i is the generalised coordinate variables and $L=T_E-U_E$ is the Lagrangian equation. Also, Q_i shows the generalised forces and moments. T_E is the total kinetic energy, U_E is the potential energy resulted from springs elements and U_D is the damping potential. The kinetic and potential energy and damping potential equations are derived as

$$T_E=\frac{1}{2}\left(\begin{array}{l}\left(m_{11}\dot{z}_{11}{}^2+m_{11}\dot{y}_{11}{}^2+I_{x11}\dot{\theta}_{x11}{}^2+I_{y11}\dot{\theta}_{y11}{}^2+I_{z11}\dot{\theta}_{z11}{}^2\right)\\+\sum_{i=1}^{2}m_{2i}\dot{z}_{2i}{}^2+m_{2i}\dot{y}_{2i}{}^2+I_{vx2i}\dot{\theta}_{x2i}{}^2+I_{vy2i}\dot{\theta}_{y2i}{}^2+I_{vz2i}\dot{\theta}_{z2i}{}^2\end{array}\right) \tag{2}$$

$$U_E=\frac{1}{2}\left(\sum_{i=1}^{2}\sum_{j=1}^{2}\sum_{n=1}^{2}\left\{\begin{array}{l}K_{1ijn}R_{1ijn}{}^2\delta_{1j}+K_{2ijn}R_{2ijn}{}^2\\+K_{3ijn}R_{3ijn}{}^2+K_{4ijn}R_{4ijn}{}^2\delta_{1j}\end{array}\right\}+\sum_{i=1}^{2}K_{5i11}R_{5i11}{}^2\right) \tag{3}$$

$$U_D=\frac{1}{2}\left(\sum_{i=1}^{2}\sum_{j=1}^{2}\sum_{n=1}^{2}\left\{\begin{array}{l}C_{1ijn}\dot{R}_{1ijn}{}^2\delta_{1j}+C_{2ijn}\dot{R}_{2ijn}{}^2\\+C_{3ijn}\dot{R}_{3ijn}{}^2+C_{4ijn}\dot{R}_{4ijn}{}^2\delta_{1j}\end{array}\right\}+\sum_{i=1}^{2}C_{5i11}\dot{R}_{5ijn}{}^2\right) \tag{4}$$

where i is stating the suspension position ($i=1$; front, $i=2$; rear), the subscript j is the tyre location in the bogie, n is expressing the left and right side of the vehicle ($n=1$; right, $n=2$; left). Also, R_{1ijn}, R_{2ijn}, R_{3ijn}, R_{4ijn} and R_{5ijn} are the relative displacements at spring/damper locations. These deformations are described in equations (5)–(9).

$$R_{1ijn}=z_{11}-(-1)^n\theta_{x11}L_{vy2}-(-1)^i\theta_{y11}L_{vxi}-(z_{2i}-(-1)^n\theta_{x2i}L_{y2}) \tag{5}$$

$$R_{2ijn}=z_{2i}-(-1)^n\theta_{x2i}L_{vy4}-(-1)^j\theta_{y2i}L_{x3}-V_{2ijn} \tag{6}$$

$$R_{3ijn}=y_{2i}+\theta_{x2i}\left(L_{z3}+L_{z4}\right)+(-1)^j\theta_{z2i}L_{x4}-V_{3ijn} \tag{7}$$

$$R_{4ijn}=y_{2i}+\theta_{vx2i}\left(L_{z3}+L_{z4}+L_{z5}\right)-V_{4ijn} \tag{8}$$

$$R_{5ijn}=y_{11}+\theta_{x11}L_{z1}+(-1)^i\theta_{z11}L_{xi}-y_{2i} \tag{9}$$

Appendix B gives details on the governing equation, including centrifugal forces, for the modelled monorail vehicle.

3 MR damper modelling

There are several mathematical models to describe the dynamic behaviour of the MR fluid damper (Spencer et al., 1997; Choi et al., 2001; Sakai et al., 2003). In this study modified dynamic LuGre friction model that exhibits hysteresis effect and the damping

force by fewer parameters is used. Damper force is predicted by using inputs of the relative velocity, $\dot{x}_{mr}$, the inner state, z, and the control voltage to the MR damper, v.

Mathematical force equation of the LuGre model is defined as follows

$$f = \sigma_a z + \sigma_0 z v - \sigma_1 a_0 \left|\dot{x}_{mr}\right| z + (\sigma_1 + \sigma_2)\dot{x}_{mr} + \sigma_b \dot{x}_{mr} v \tag{10}$$

For control design purposes, the force equation given in (10) can also be written in the following form

$$f = \begin{bmatrix} z & vz & -\left|\dot{x}_{mr}\right| z \end{bmatrix} \begin{bmatrix} \sigma_a \\ \sigma_0 \\ \sigma_1 a_0 \end{bmatrix} + \begin{bmatrix} \dot{x}_{mr} & \dot{x}_{mr} v \end{bmatrix} \begin{bmatrix} \sigma_1 + \sigma_2 \\ \sigma_b \end{bmatrix} \tag{11}$$

where z, v and $\dot{x}_{mr}$ are matrices whose elements correspond to each MR damper value

$$\begin{aligned} z &= \mathrm{diag}\begin{pmatrix} z_{FR} & z_{FM} & z_{FL} & z_{RR} & z_{RM} & z_{RL} \end{pmatrix} \\ v &= \mathrm{diag}\begin{pmatrix} v_{FR} & v_{FM} & v_{FL} & v_{RR} & v_{RM} & v_{RL} \end{pmatrix} \\ \dot{x}_{mr} &= \mathrm{diag}\begin{pmatrix} \dot{x}_{FR} & \dot{x}_{FM} & \dot{x}_{FL} & \dot{x}_{RR} & \dot{x}_{RM} & \dot{x}_{RL} \end{pmatrix} \end{aligned} \tag{12}$$

MR damper parameters can be separated as right, middle and left such as

$$\begin{aligned} \sigma_a &= \begin{bmatrix} \sigma_{a_{FR}} & \ldots & \sigma_{a_{RL}} \end{bmatrix}^T \qquad \sigma_0 = \begin{bmatrix} \sigma_{0_{FR}} & \ldots & \sigma_{0_{RL}} \end{bmatrix}^T \\ \sigma_b &= \begin{bmatrix} \sigma_{b_{FR}} & \ldots & \sigma_{b_{RL}} \end{bmatrix}^T \quad \sigma_1 a_0 = \begin{bmatrix} (\sigma_1 a_0)_{FR} & \ldots & (\sigma_1 a_0)_{RL} \end{bmatrix}^T \\ \sigma_1 + \sigma_2 &= \begin{bmatrix} (\sigma_1 + \sigma_2)_{FR} & \ldots & (\sigma_1 + \sigma_2)_{RL} \end{bmatrix}^T \end{aligned} \tag{13}$$

Equation (11) can be rewritten as

$$f = \rho_1 \theta_1 + \rho_2 \theta_2 \tag{14}$$

where MR damper parameter vectors θ_1, θ_2 and the input signals ρ_1, ρ_2 are defined as

$$\begin{aligned} \rho_1 &= \begin{bmatrix} z & vz & -\left|\dot{x}_{mr}\right| z \end{bmatrix} \qquad \rho_2 = \begin{bmatrix} \dot{x}_{mr} & \dot{x}_{mr} v \end{bmatrix} \\ \theta_1 &= \begin{bmatrix} \sigma_a & \sigma_0 & \sigma_1 a_0 \end{bmatrix}^T \quad \theta_2 = \begin{bmatrix} \sigma_1 + \sigma_2 & \sigma_b \end{bmatrix}^T \end{aligned} \tag{15}$$

In this study, two semi-active control approaches are studied for applying calculated control voltage to the MR dampers. First one is the saturation method (used in adaptive control) that the calculated control signals are trimmed to be within a permissible limit of the MR damper. The second one (used in H_∞ control) is comparing real and calculated damper force by the inverse model of the MR damper equation given in equation (16) to obtain a required control voltage

$$v_{\inf} = \frac{f_c - \left\{\sigma_a z - \sigma_1 a_0 \left|\dot{x}\right| z + (\sigma_1 + \sigma_2)\dot{x}\right\}}{\sigma_0 z + \sigma_b \dot{x}} \tag{16}$$

where f_c is the desired control force calculated by the H_∞ controller.

4 H_∞ control design

In H_∞ control design, it is desired to synthesise a controller $K_\infty(s)$ with the input u and output y, such that the closed loop is stabilised, and the performance output z is minimised, given a class of disturbance inputs w. The transfer matrix from the system disturbance w to the controlled output z is obtained as

$$z = T_{zw}(s)w \tag{17}$$

The H_∞ control design objective is to obtain a controller that minimises the infinity norm of the closed loop transfer matrix such as

$$\left\|T_{zw}(s)\right\|_\infty < \gamma \tag{18}$$

where $\gamma > 0$. The generalised control design block structure of the H_∞ control is shown in Figure 3.

Figure 3 Generalised system structure

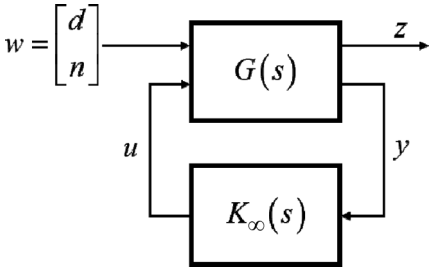

Figure 4 Schematic diagram of the monorail control system structure (see online version for colours)

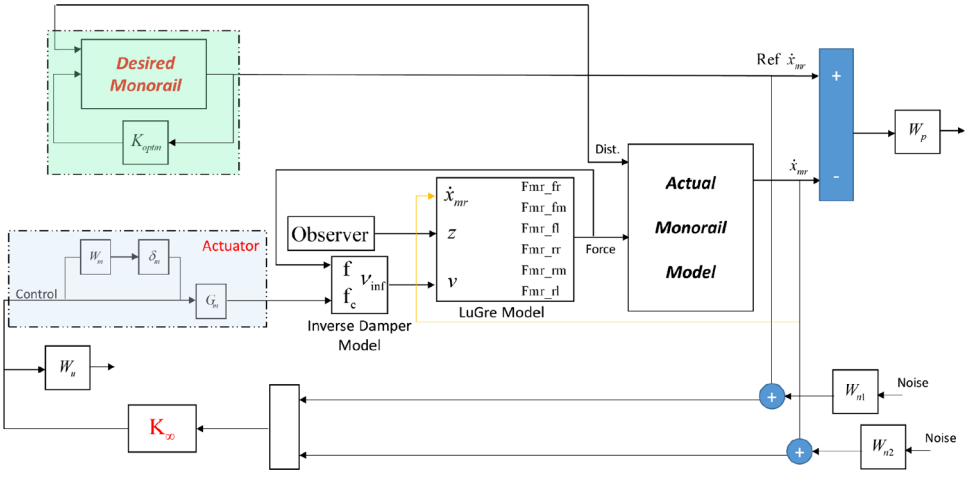

H_∞ control approach has been widely applied in suspension control of railway vehicles (Yıldız et al., 2015; Orvnäs et al., 2011). In the proposed H_∞ control design, the controller inputs are selected as both velocities of the MR dampers of the desired and actual model. The desired monorail vehicle is assumed to have an optimal suspension

system. Moreover, H_∞ controller produces requested damper velocities to feed the assumed actuator model. By this way, an optimal control force can be calculated for the inverse MR damper model to generate a control voltage. This approach is summarised in Figure 4. In the control system structure, weighting filters are shown for better understanding the implementation points.

4.1 MR damper model with multiplicative uncertainty

By assuming uncertainties in MR dampers, nonlinear effects and variations of model parameters due to in-service conditions can be modelled more realistically. Uncertainties are approximated by input multiplicative uncertainties as shown in equation (19).

$$\bar{G}_m = (1 + W_m \delta_m) G_m \tag{19}$$

Determining $W_m(j\omega)$ is equivalent to finding of the upper bound of the magnitude response of relative error (Gu et al., 2014). The filter $W_m(j\omega)$ is chosen as

$$W_m(s) = \frac{0.2371s + 120.1}{s + 1149} \tag{20}$$

The mathematical model of the MR damper used in this study is nonlinear. To incorporate the suspension model into system dynamics, MR dampers are assumed as a first order phase-lag model transfer function

$$G_m(s) = \frac{1360}{0.001s + 1} \tag{21}$$

Using the transfer function approach, it is possible to realise the nonlinear force output of the MR damper in an acceptable level throughout the road profile as seen in Figure 5.

Figure 5 Transfer function approximation of the force output (see online version for colours)

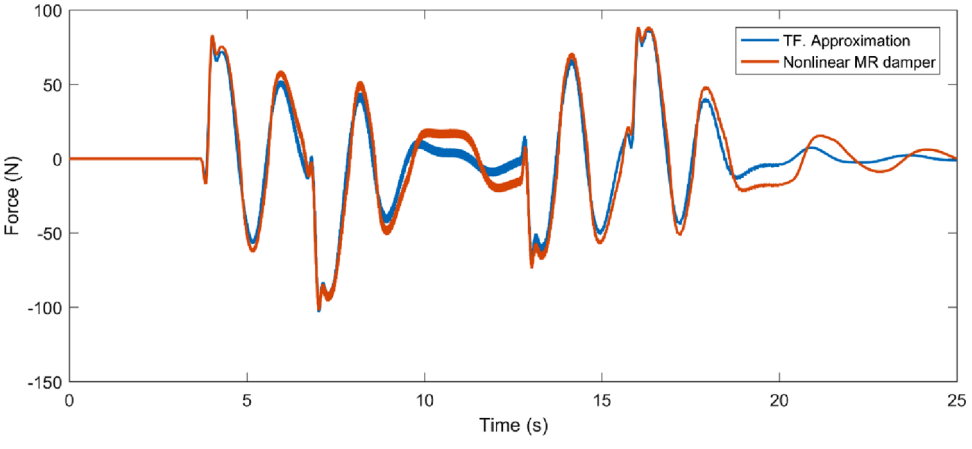

4.2 Weighting transfer function for sensor noises

In robust control applications, sensor noises should also be considered to improve the output performance of the control system. The transfer function of the weighting filter for

sensor noise is selected as a high-pass filter and arranged in diagonal form for the control design. Measurement error about 0.001 V is assumed in the low-frequency range and 0.1 V measurement error in the high-frequency range by this transfer function

$$W_n(s) = \begin{bmatrix} w_n & & & & & & \\ & w_n & & & & & \\ & & w_n & & & & \\ & & & w_n & & & \\ & & & & w_n & & \\ & & & & & w_n & \end{bmatrix}, \quad w_n(s) = 1\text{x}10^{-3}\,\frac{10s+1}{0.1s+1} \tag{22}$$

Figure 6 Inverse frequency responses of performance weighting filters (see online version for colours)

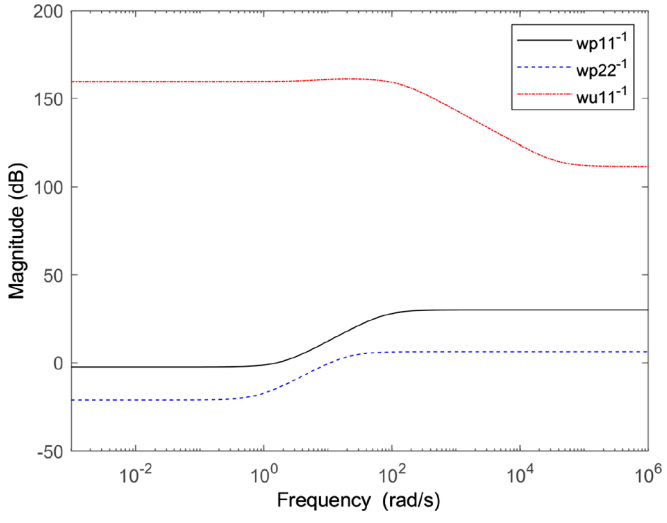

4.3 Selection of the performance filters

In H_∞ control design, weighting functions are applied to the input and output signals of the system to define the amount of influence each signal should have in the calculation of the controller (Orvnäs et al., 2011). In our design, the objectives of the controller are aimed to reduce MR dampers working velocity difference between desired and actual model. For this purpose, six low-pass performance weighting filters are introduced in the control design, $W_p = \text{diag}(1/w_{p11}, 1/w_{p22}, 1/w_{p11}, 1/w_{p11}, 1/w_{p22}, 1/w_{p11})$. Here, filters for front and rear damper sets are selected as same. The weighting filter w_{p11} is designed for the MR dampers placed in the right and left side and w_{p22} is for the lateral damper in the front and rear bogies.

$$w_{p11}(s) = \frac{31.88s + 59.48}{s + 78.11}, \quad w_{p22}(s) = \frac{2.068s + 1.735}{s + 19.66} \tag{23}$$

The control force in high-frequency range could not be easily followed by the MR damper because of the time delay, thus a high-pass transfer function is introduced for the

weighting control force as $W_u = 1\text{x}10^{-5}\,\text{diag}(1/w_{u11}, 1/w_{u11}, 1/w_{u11}, 1/w_{u11}, 1/w_{u11}, 1/w_{u11})$. Frequency responses of these filters can be seen in Figure 6.

$$w_{u11}(s) = \frac{3.782s^2 + 1.465\text{x}10^5 s + 8.422\text{x}10^5}{s^2 + 132.8s + 878.7} \tag{24}$$

5 Adaptive control design

In a previous research study of Yıldız et al. (2015), a nonlinear adaptive controller was designed, and its application was performed experimentally on a suspension system of the quarter car vehicle model. In the mentioned study, only one MR damper was used and just the vertical dynamics was considered. Same control framework is extended for the monorail vehicle, so all MR dampers placed on the front and rear bogies in vertical and lateral direction can be controlled at the same time. The control design begins by defining an error variable

$$e = x_s - x_{sd} \tag{25}$$

When a filtered error signal r is introduced to incorporate the monorail equation of motion defined in (B4)

$$r = \dot{e} + \alpha e \tag{26}$$

Here α is a constant, diagonal and positive definite gain matrix. The main objective of the controller is regulation of $r(t)$ to adjust both $x_s(t)$ and $\dot{x}_s(t)$. When the system equations given in Appendix (B4) is incorporated into the derivative of equation (26), the error dynamics can be obtained as follows

$$\begin{aligned} M\dot{r} &= M\left(\ddot{x}_s + \alpha\dot{x}_s\right) = M\alpha\dot{x}_s - C\dot{x}_s - Kx_s - LF_{dist} - Hf \\ &= \psi\phi - Hf \end{aligned} \tag{27}$$

where ψ is a matrix and consists of known and measurable signals and ϕ is the unknown system parameter vector includes mass, inertia, stiffness and damping coefficients of the system.

$$\psi = \begin{bmatrix} \psi_m & \psi_c & \psi_k \end{bmatrix} \quad \phi = \begin{bmatrix} \phi_m & \phi_c & \phi_k \end{bmatrix} \tag{28}$$

Here unknown parameters are given as

$$\begin{aligned} \phi_m &= \begin{bmatrix} m_{ii} & I_{zii} & I_{yii} & I_{xii} \end{bmatrix}^T_{12x1} \\ \phi_c &= \begin{bmatrix} C_{1ijn} & C_{2ijn} & C_{3ijn} & C_{4ijn} \end{bmatrix}^T_{26x1} \\ \phi_k &= \begin{bmatrix} K_{1ijn} & K_{2ijn} & K_{3ijn} & K_{4ijn} \end{bmatrix}^T_{26x1} \end{aligned} \tag{29}$$

The MR damper force equation given in (14) contains unknown parameters; therefore, it cannot be used directly. Instead of using (14), equation (27) is rewritten by adding and subtracting the estimated force expression $H\hat{f}$ that is explained in (B8) to (B10). The filtered error dynamics becomes as follows

$$\begin{aligned} M\dot{r} &= \psi\phi + H\chi - Hu - H\left(\rho_1\theta_1 + \rho_2\theta_2 - \hat{\rho}_1\hat{\theta}_1 - \rho_2\hat{\theta}_2\right) \\ &= \psi\phi + H\chi - Hu - H\rho_2\tilde{\theta}_2 \\ &\quad - H\left(\theta_{11}z - \hat{\theta}_{11}\hat{z} + \theta_{12}z - \hat{\theta}_{12}v\hat{z} - \theta_{13}\left|\dot{x}_{mr}\right|z + \hat{\theta}_{13}\left|\dot{x}_{mr}\right|\hat{z}\right) \end{aligned} \tag{30}$$

For calculation simplicity, χ and u are defined as

$$\chi = -\hat{\theta}_{11}\hat{z} + \hat{\theta}_{13}\left|\dot{x}_{mr}\right|\hat{z} - \hat{\theta}_{21}\dot{x}_{mr}, \quad u = \left(\hat{\theta}_{12}\hat{z} + \hat{\theta}_{22}\dot{x}_{mr}\right)v \tag{31}$$

From the result of the stability analysis that explained detailed in the study (Yıldız et al., 2015), the control input u was designed in the form of

$$Hu = Kr + H\chi + \psi\phi + H\left(-\hat{\theta}_{11}\zeta_1 - \hat{\theta}_{12}\zeta_2 v + \hat{\theta}_{13}\left|\dot{x}_{mr}\right|\zeta_3\right) \tag{32}$$

Input voltages to each MR damper can be calculated by using equation (32) and given in equation (33). The sequence of the control voltage signal is given in equation (12).

$$Hv = \frac{Kr + H\chi + \psi\phi + H\left(-\hat{\theta}_{11}\zeta_1 + \hat{\theta}_{13}\left|\dot{x}_{mr}\right|\zeta_3\right)}{\left(\hat{\theta}_{12}\hat{z} + \hat{\theta}_{22}\dot{x}_{mr} + \hat{\theta}_{12}\zeta_2\right)} \tag{33}$$

It is better to compare both the H_∞ and adaptive control design approaches to understand the differences. In the H_∞ control approach, an uncertain actuator model that corresponding to the MR damper and uncertain system parameters are used to construct the uncertain monorail system. The desired system and the closed loop system closeness is ensured by frequency dependent weighting functions. Also, the output of the H_∞ controller should be converted to a control voltage by an inverse model defined in equation (16). However, the adaptive controller calculates the control voltage directly.

6 Road design

A moving coordinate system is usually used in the curving simulation of a rail vehicle (Pombo and Ambrósio, 2003; Shaltout et al., 2015). In this approach, the position of the coordinates is defined with respect to the track centreline. In literature, there are some track centreline parameterisation methods such as analytical segments, and cubic splines (Shaltout et al., 2015). In analytical segments procedure, the track is built using a combination of straight, transition and circular curve segments as seen in Figure 7.

Straight line stage: Monorail vehicle is firstly run on $\sigma = 50$ m straight segment.

Transition curve stage: In the designed road profile, $\sigma = 30$ m a clothoid curve is used to enable a gradual transition in lateral acceleration. Components of the road in all directions are obtained by equation (34) with respect to road distance σ.

$$p_T(\sigma)=\begin{bmatrix} x_t(\sigma) \\ y_t(\sigma) \\ z_t(\sigma) \end{bmatrix}=\begin{bmatrix} \sigma-\dfrac{1}{10}\dfrac{\sigma^5}{\pi^2}\kappa^2 \\ \dfrac{1}{6}\sigma^3\kappa-\dfrac{1}{84}\dfrac{\sigma^7}{\pi^2}\kappa^3 \\ \dfrac{h_{\max}-h_{\min}}{l_{clo}}\sigma \end{bmatrix} \tag{34}$$

where κ is a constant and it can be calculated as

$$\kappa=\frac{1}{l_{clo}R} \tag{35}$$

Here, l_{clo} is the length of the transition stage, $h_{\max}$ and $h_{\min}$ are the initial and final super elevation value of the stage, respectively.

Circular curve stage: In this stage, the vehicle runs on 206 m in length with a constant radius of curvature $R=150\,\text{m}$. Equation (36) describes the circular road components.

$$p_C(\sigma)=\begin{bmatrix} x_{cir}(\sigma) \\ y_{cir}(\sigma) \\ z_{cir}(\sigma) \end{bmatrix}=\begin{bmatrix} \left(\sin\left(\sigma/R+\Phi_i\right)-\sin\left(\Phi_i\right)\right)R+x_i \\ \left(-\cos\left(\sigma/R+\Phi_i\right)+\cos\left(\Phi_i\right)\right)R+y_i \\ h_{t\max} \end{bmatrix} \tag{36}$$

The variable Φ_i is the clothoid angle at the end of the transition which is described by equation (37).

$$\Phi(\sigma)=\arctan\left(\frac{\mathrm{d}y/\mathrm{d}\sigma}{\mathrm{d}x/\mathrm{d}\sigma}\right) \tag{37}$$

Transition and straight segments are again following the same order but decreasing super elevation after circular curve as given in Figure 8.

Figure 7 Top view of the designed road profile for simulations

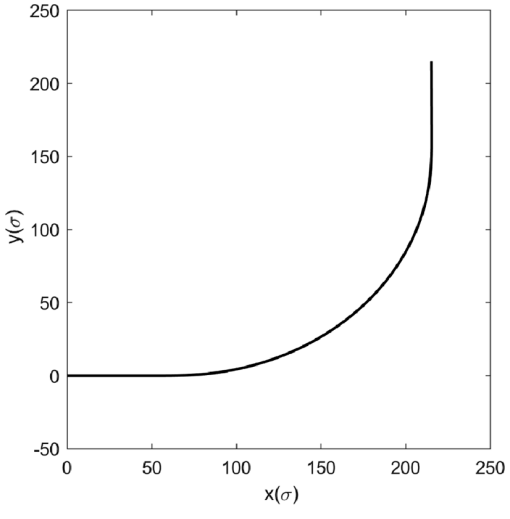

Figure 8 Curvature and cant of the road profile

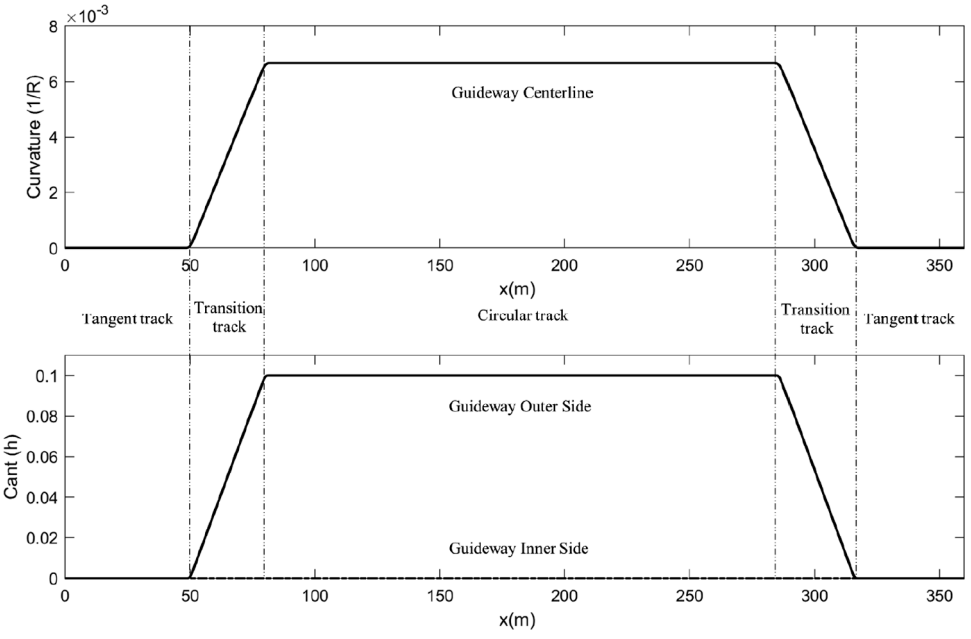

7 Simulation results

The effectiveness of the proposed H_∞ and adaptive controllers are tested in the Matlab-Simulink environment. The performances of the designed controllers are compared with the uncontrolled (MR damper is not connected) and the passive (MR damper is connected but no electricity is supplied) cases. Since a single MR damper cannot produce a sufficient damping force, a set of two MR dampers are used. The parameters used in simulations of the monorail vehicle are taken from the study conducted by Lee et al. (2005) and the parameter of the Lord 1005-3 MR damper values are given in Table 2.

Table 2 The parameter of the Lord 1005-3 MR damper

Parameters	*Definitions*	*Values*	*Units*
σ_0	Stiffness of $z(t)$ influenced by $v(t)$	320,000	N/(m.V)
σ_1	Damping coeff. of $z(t)$	3.21	N.s/m
σ_2	Viscous damping coeff. influenced by $v(t)$	1153.3	N.s/m
σ_a	Stiffness of $z(t)$	10,000	N/m
σ_b	Viscous damping coeff. influenced by $v(t)$	315	N.s/(m.V)
a_0	Constant value	1400	V/N

The frequency response from the front right running tyre to the velocity of the front right vertical MR damper for the open-loop, H_∞ control, adaptive control and the inverse of

the selected filters are shown in Figure 9. The control objective is reducing the resonance peak for low and high frequencies and these criteria are achieved.

Figure 9 The frequency response of the controller from the front right running tyre to the relative velocity of the front right vertical MR damper (see online version for colours)

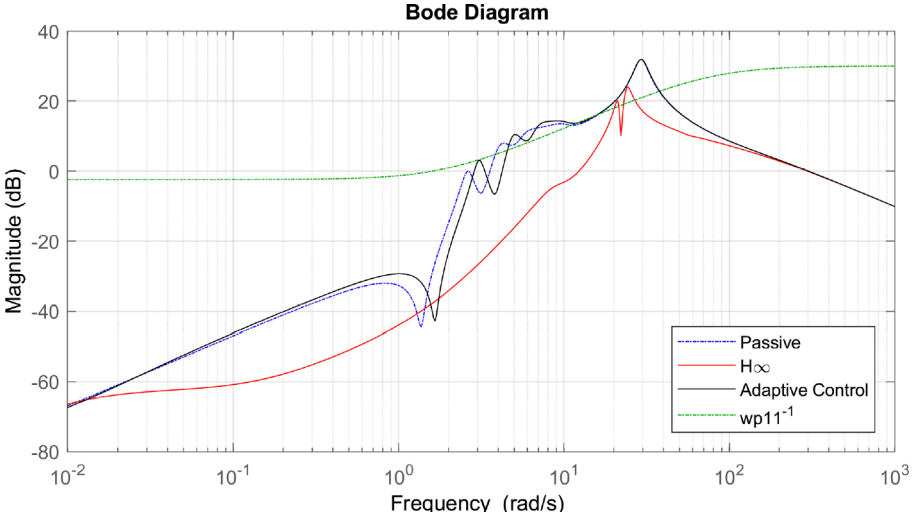

Table 3 RMS and peak to peak values of the monorail body accelerations (unit: vertical, lateral – m/s^2, roll – rad/s^2, yaw – rad/s^2)

	RMS values			*Peak to peak values*		
	Passive	H_∞	*Adaptive*	*Passive*	H_∞	*Adaptive*
$\ddot{z}_{11}$	0.014	0.011	0.019	0.112	0.149	0.377
$\ddot{y}_{11}$	0.195	0.152	0.142	3.933	3.921	4.058
$\ddot{\theta}_{x11}$	0.173	0.123	0.113	1.563	1.524	1.306
$\ddot{\theta}_{z11}$	0.014	0.014	0.014	0.221	0.215	0.247
Reduction ($\ddot{z}_{11}$)%	49.47	79.66	6.036	32.88	–0.83	–60.60
Reduction ($\ddot{y}_{11}$)%	34.09	73.23	85.04	0.57	0.88	–2.54
Reduction ($\ddot{\theta}_{x11}$)%	41.13	97.87	115.47	7.32	10.06	28.50
Reduction ($\ddot{\theta}_{z11}$)%	2.27	2.32	2.52	2.43	4.86	–8.45

The root-mean-square (RMS) and peak-to-peak values of the monorail body accelerations during the curving are obtained for the H_∞ control, adaptive control and passive case and the results are shown in Table 3. Also, the reduction is given in percent relative to the uncontrolled case. Negative reduction means the deterioration in performance index. RMS value for the vehicle body acceleration is given in equation (38).

$$J_1 = \sqrt{\frac{1}{N}\sum_{n=1}^{N}\left|\ddot{z}_{11}(t)\right|^2}, J_2 = \sqrt{\frac{1}{N}\sum_{n=1}^{N}\left|\ddot{y}_{11}(t)\right|^2}, J_3 = \sqrt{\frac{1}{N}\sum_{n=1}^{N}\left|\ddot{\theta}_{x,z11}(t)\right|^2} \tag{38}$$

According to Table 3, it is observed that the adaptive controller reduced the RMS value of the roll acceleration to 115% as compared to the uncontrolled case but increased vertical acceleration peak to peak value to 60%. This is due to the fact that the adaptive controller is designed to minimise displacement which causes undesirable peak acceleration.

As seen in Figures 10 and 11, vibration reduction ability of the semi-active suspension with the proposed control approaches are better than that of the passive suspension. Also, the adaptive controller can reduce the car body roll acceleration better than the passive and H_∞ control cases as given in Table 3. Also, oscillations after the circular curve are eliminated. Improvement in the lateral motion of the vehicle also affects positively the vehicle rolling motion, this effect can be seen in Figure 10. Reduction in both rolling and lateral acceleration improve curving performance of the monorail vehicle.

Figure 10 Vehicle body roll acceleration (see online version for colours)

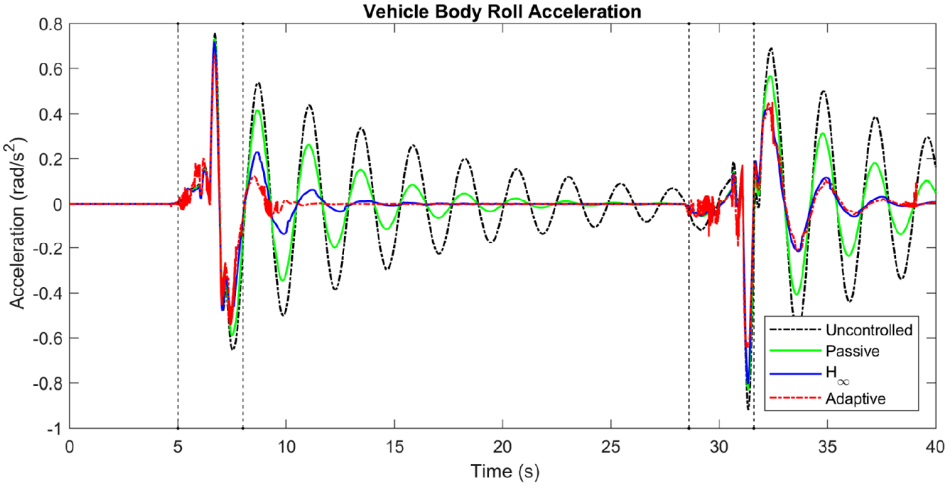

Figure 11 Vehicle body lateral acceleration (see online version for colours)

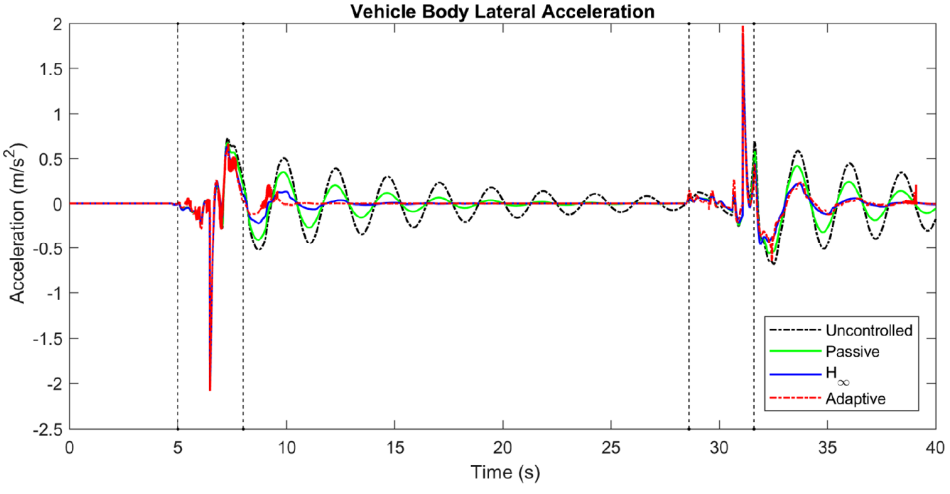

The proposed control approaches reduce the vertical displacement of the monorail body displacements both entering the curve and leaving the curve as shown in Figure 12. Also, vibrations during the circular curve occur between 8th and 28.8th second are diminished. This improvement ends up with deterioration in vertical peak acceleration as seen in Table 3, also the same adverse effect can be seen in the vertical comfort value in Section 7.2. However, H_∞ control can achieve decrement in both displacement and comfort index values. As seen in Figure 13, the vehicle body yaw angle changes with the second bogie entrance and exit of the transition track segment.

Figure 12 Vehicle body vertical displacement (see online version for colours)

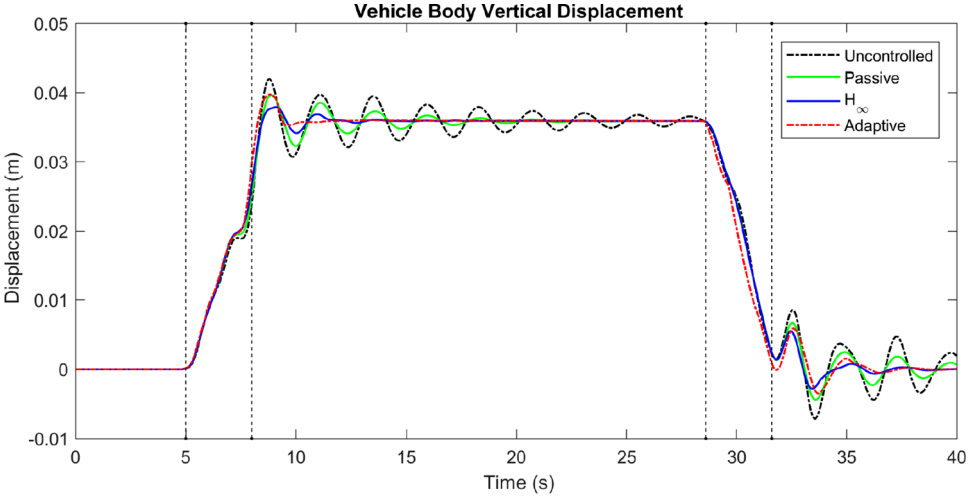

Figure 13 Vehicle body yaw angle (see online version for colours)

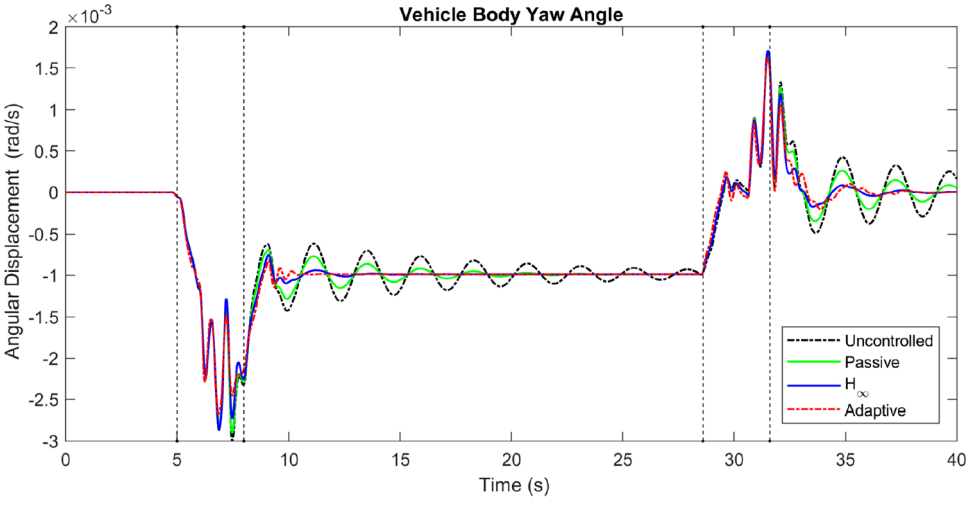

Figure 14 shows the time histories of the desired and actual forces of the H_∞ control. The desired force is the force output of the reference system with optimal static feedback gain as defined in Appendix A. It can be seen in Figure 14 that required force

(expressed by a black dash-dot line) and the force produced by MR dampers with the H_∞ controller are the same. It means that the required force is reproducible by the MR dampers. Also, the adaptive controller achieves better performance with almost the same force level.

Figure 14 Force output of the MR damper placed at the left side of the front bogie (see online version for colours)

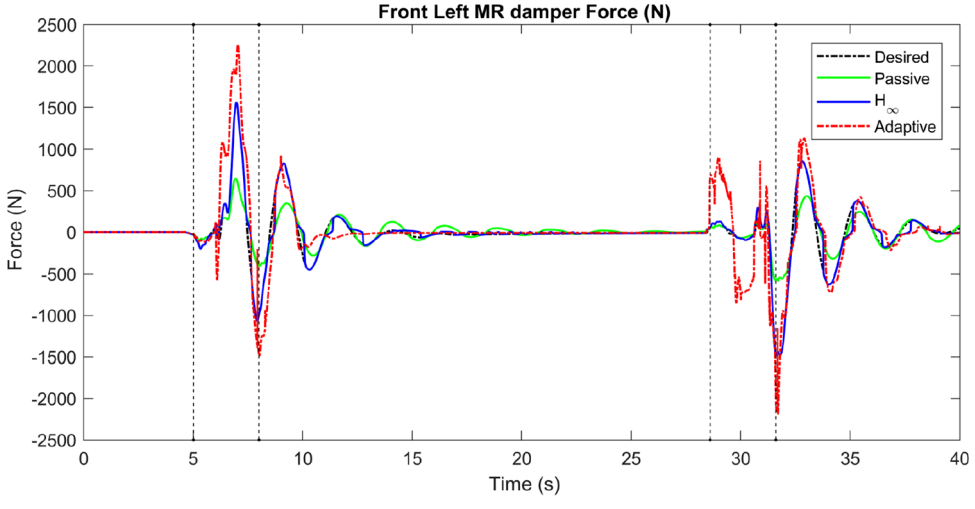

7.1 Comparison of curving performance

Curving performance is evaluated by using the bogie lateral displacement. As seen in Figure 15, the peak value of the front bogie lateral displacement is decreased with the designed controllers. This decrement may also provide an extended service life to running tyres because the lower lateral displacements cause lower abrasion on tyres. Also, the vertical load acts on the tyre contact surface is a rational cause of wear. Higher loads make greater deformations on tyre treads which causes wear.

7.2 Comparison of ride comfort

Ride comfort is measured by some specific indices by considering acceleration level, frequency, direction, and location. The International Standard (ISO 2631-1, 1997) specifies a method of evaluation of the effect exposure to vibration on humans by weighting RMS acceleration with human vibration-sensitivity curves.

$$a_w = \left[\frac{1}{T} \int_0^T a_w{}^2(t)\, dt \right]^{\frac{1}{2}} \tag{39}$$

where, a_w is the weighted acceleration as a function of time in meters per second squared (m/s^2) and T is the duration of the measurement, in seconds.

In this study, road roughness is not considered therefore all cases are in the *comfortable* limit of the scale that defined by ISO 2631. The weighted RMS values of the overall comfort index are summarised in Table 4. As seen in Table 4, the adaptive control

serves better comfort in the lateral direction but result in deterioration in the vertical comfort value. This is because the adaptive control is designed to minimise values defined in Table 1.

Figure 15 Front bogie inner side running tyre lateral displacement and vertical force (see online version for colours)

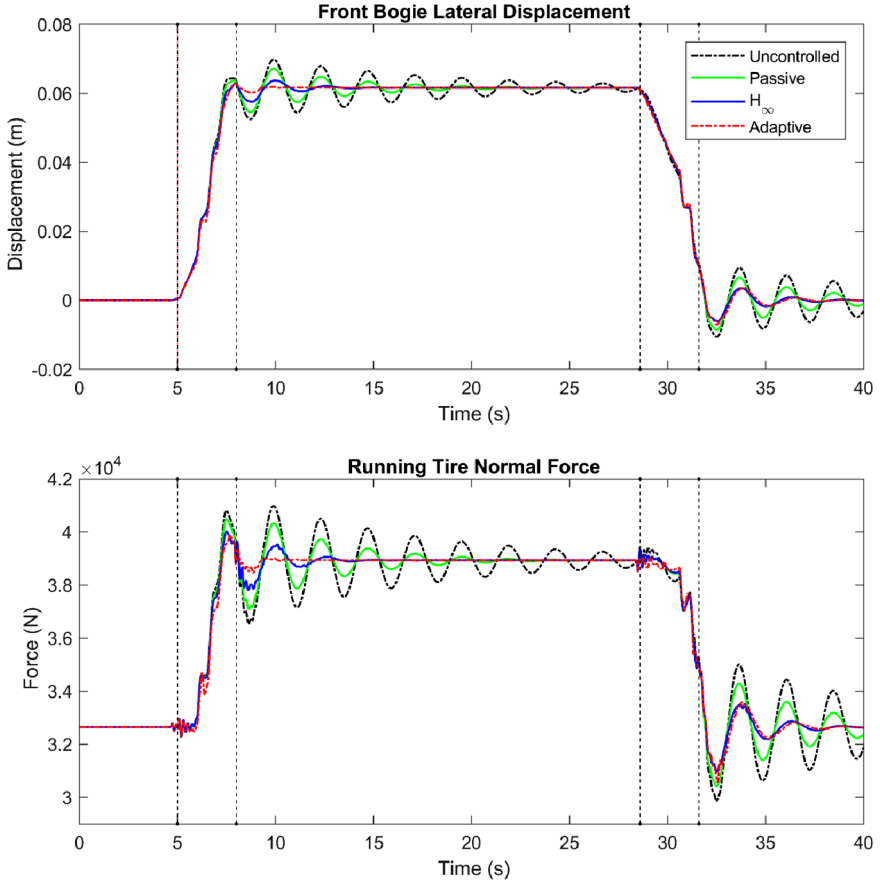

Table 4 Effect of the control approaches on ride comfort: weighted RMS values (m/s^2)

	Uncontrolled	*Passive*	*H_∞ control*	*Adaptive control*
Vertical	0.0085	0.0058	0.0055	0.0081
Lateral	0.1951	0.1466	0.1141	0.1032

Figure 16. shows the vertical and lateral comfort index calculated at 1 s intervals. Both vertical and lateral comfort indices are majorly influenced by the transition track segment. One can see that the H_∞ control provides better the vertical comfort when compared to other cases but the adaptive control achieves better lateral comfort.

Figure 16 Vertical and lateral comfort values (see online version for colours)

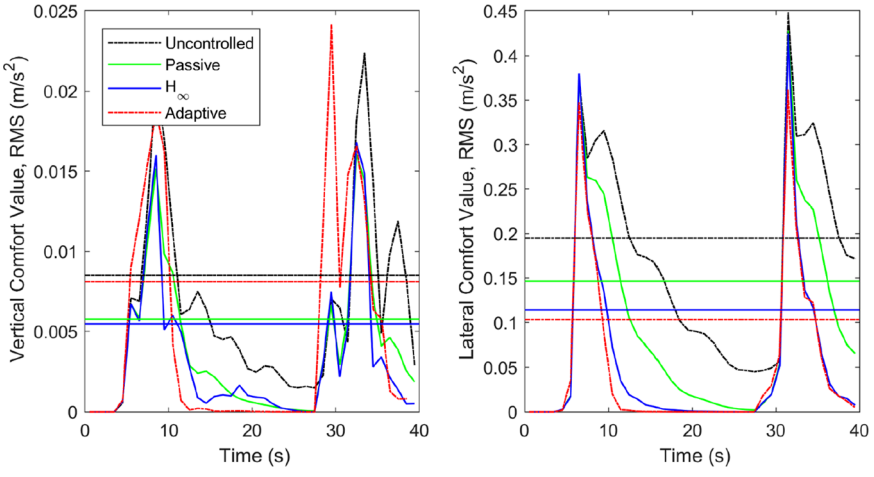

7.3 Adaptation performance

In monorail vehicles, running on rubber tyres causes abrasion. Also, existing uncertainties in a monorail vehicle influence the performance of suspension systems. Therefore, system parameters related to tyre dynamics should be modelled considering these uncertainties.

Figure 17 Estimation behaviour of the monorail mass values to their true values (see online version for colours)

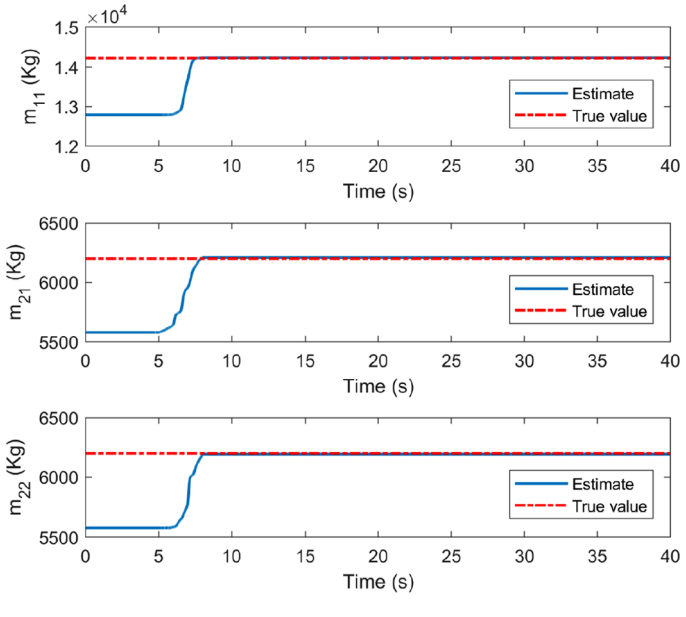

In the designed adaptive control, mass, damping and stiffness parameters are guaranteed to converge to their true values under a persistent excitation condition when associated

adaptation gain is adjusted. In the adaptive and H_∞ control design, we assume 10% uncertainties in mass properties and 15% uncertainties in running tyre parameters (both damping and stiffness properties) because of that running tyres run under higher abrasion condition. The convergence behaviour is summarised in Figures 17 and 18.

Figure 18 Estimation of the damping and stiffness parameters to their real values (see online version for colours)

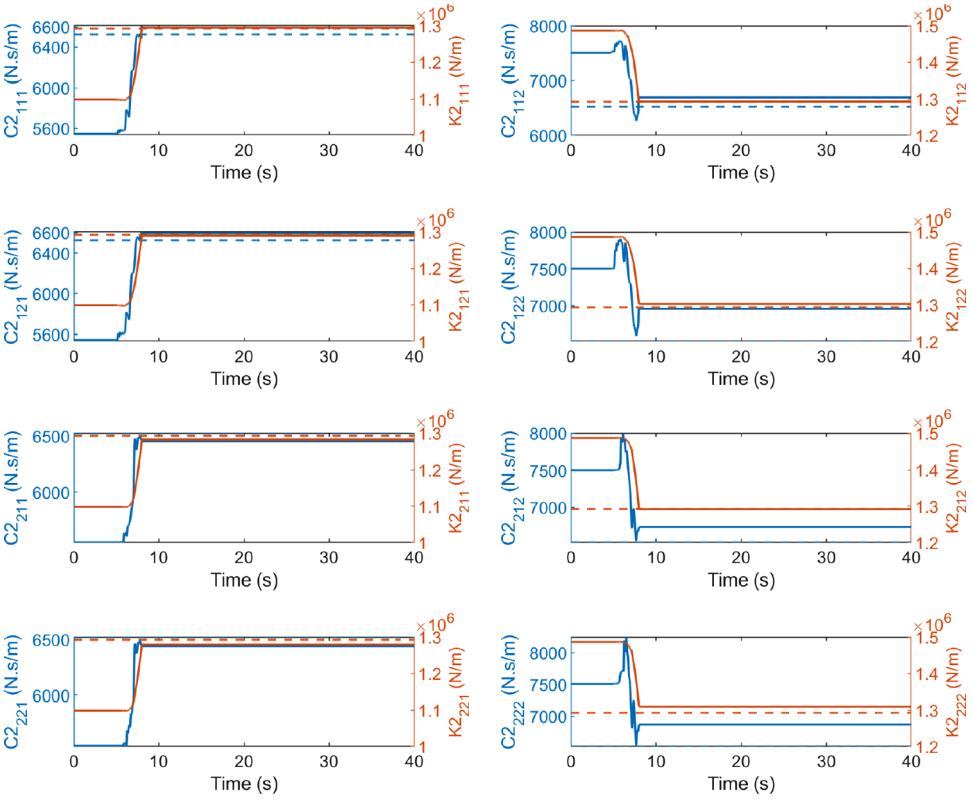

8 Conclusions

A simulation structure is developed for a full-scale monorail vehicle that equipped with the semi-active suspension. Changing vehicle mass, tyre wear, and guideway misalignments should be considered in monorail suspension designing. Therefore, parametric uncertainties are considered in proposed control techniques.

Ride comfort of the monorail vehicle was evaluated with respect to ISO 2631:1997. Results show that semi-active suspension in conjunction with proper control approaches provides better comfort and stability. Also, an adaptive controller that comprises an algorithm for updating the monorail vehicle parameters which is based on the Lyapunov stability theory is used and thus, the stability of the uncertain system is guaranteed.

References

Bao, Y., Li, Y. and Ding, J. (2016) 'A case study of dynamic response analysis and safety assessment for a suspended monorail system', *International Journal of Environmental Research and Public Health*, Vol. 13, No. 11, p.1121.

Choi, S.B., Lee, S.K. and Park, Y.P. (2001) 'A hysteresis model for the field-dependent damping force of a magnetorheological damper', *Journal of Sound and Vibration*, Vol. 245, No. 2, pp.375–383.

Du, Z.X., Cao, D.T., Wen, X.X. and He, Q.H. (2017) 'Study on the influence of safety of air spring failure for straddle-type monorail vehicle', *Design, Manufacturing and Mechatronics: Proceedings of the International Conference on Design, Manufacturing and Mechatronics (ICDMM2016)*, Wuhan, China, pp.371–378.

Du, Z.X., Wen, X.X. and Shen, Z. (2014) 'The impact analysis of tire parameter for tire wear when monorail vehicle curve driving', *Applied Mechanics and Materials*, Trans Tech Publications, Vol. 470, pp.529–533.

Goda, K., Nishigaito, T., Hiraishi, M. and Iwasaki, K. (1999) 'Response analysis caused by track irregularity for a monorail', *Transactions of the Japan Society of Mechanical Engineers. C.*, Vol. 65, No. 637, pp.3546–3552.

Goda, K., Nishigaito, T., Hiraishi, M. and Iwasaki, K. (2000) 'A curving simulation for a monorail car', *Railroad Conference, 2000. Proceedings of the 2000 ASME/IEEE Joint*, IEEE, Newark, NJ, USA, USA, pp.171–177.

Gu, D.W., Petkov, P.H. and Konstantinov, M.M. (2014) *Robust Control Design with MATLAB®*. Springer Science & Business Media.

Hitachi Monorail Technology Presentation (2013) Hitachi, Ltd., Rail Systems Company, September 3.

ISO 2631-1 (1997) *Mechanical Vibration and Shock – Evaluation of Human Exposure to Whole-Body Vibration–Part 1*.

Kato, M., Yamazaki, K., Amazawa, T. and Tamotsu, T. (2004) 'Straddle-type monorail systems with driverless train operation system', *Hitachi Review*, Vol. 53, No. 1, p.25.

Lee, C.H., Kim, C.W., Kawatani, M., Nishimura, N. and Kamizono, T. (2005) 'Dynamic response analysis of monorail bridges under moving trains and riding comfort of trains', *Engineering Structures*, Vol. 27, No. 14, pp.1999–2013.

Maciel, G.P. and Barbosa, R.S. (2016) 'Monorail vehicle model to study influence of tyre modelling on overall dynamics', *International Journal of Heavy Vehicle Systems*, Vol. 23, No. 4, pp.317–332.

Orvnäs, A., Stichel, S. and Persson, R. (2011) 'Active lateral secondary suspension with H∞ control to improve ride comfort: simulations on a full-scale model', *Vehicle System Dynamics*, Vol. 49, No. 9, pp.1409–1422.

Pombo, J. and Ambrósio, J.A. (2003) 'General spatial curve joint for rail guided vehicles: kinematics and dynamics', *Multibody System Dynamics*, Vol. 9, No. 3, pp.237–264.

Sakai, C., Ohmori, H. and Sano, A. (2003) 'Modeling of MR damper with hysteresis for adaptive vibration control', *42nd IEEE Conference on Decision and Control, 2003. Proceedings*, IEEE, Vol. 4, December, pp.3840–3845.

Shaltout, R., Ulianov, C. and Baeza, L. (2015) 'Development of a simulation tool for the dynamic analysis of railway vehicle-track interaction', *Transport Problems*, Vol. 10, pp.47–58.

Spencer Jr., B.F., Dyke, S.J., Sain, M.K. and Carlson, J. (1997) 'Phenomenological model for magnetorheological dampers', *Journal of Engineering Mechanics*, Vol. 123, No. 3, pp.230–238.

Wang, H., Zhu, E. and Chen, Z. (2017) 'Dynamic response analysis of the straddle-type monorail bridge–Vehicle coupling system', *Urban Rail Transit*, Vol. 3, No. 3, pp.172–181.

Wen, X.X., Du, Z.X., Zhao, D.Y., Xu, Z.Z. and Zhen, Y. (2016) 'Study on the tire uneven wear mechanism of the running wheel of monorail vehicles', *Journal of Applied Science and Engineering*, Vol. 19, No. 4, pp.459–470.

Yıldız, A.S., Sivrioğlu, S., Zergeroğlu, E. and Çetin, Ş. (2015) 'Nonlinear adaptive control of semi-active MR damper suspension with uncertainties in model parameters', *Nonlinear Dynamics*, Vol. 79, No. 4, pp.2753–2766.

Zong, L.H., Gong, X.L., Xuan, S.H. and Guo, C.Y. (2013) 'Semi-active H∞ control of high-speed railway vehicle suspension with magnetorheological dampers', *Vehicle System Dynamics*, Vol. 51, No. 5, pp.600–626.

Appendix A

Monorail vehicle parameters

Definition	*Notation*	*Values*	*Units*
Mass of body	m_{11}	14.22	ton
Mass of bogies	m_{21} , m_{22}	6.20	ton
Spring constant of vertical air suspension	$K1_{ijn}$	60	kN/m
Spring constant of running tyre	$K2_{ijn}$	5170/4	kN/m
Spring constant of guide tyre	$K3_{ijn}$	6370/4	kN/m
Spring constant of stabilising tyre	$K4_{i1n}$	6370/4	kN/m
Spring constant of lateral air suspension	$K5_{i11}$	38	kN/m
Damping constant of vertical air suspension	$C1_{ijn}$	1.5	kN.s/m
Damping constant of running tyre	$C2_{ijn}$	26.1/4	kN.s/m
Damping constant of guide tyre	$C3_{ijn}$	185.5/4	kN.s/m
Damping constant of stabilising tyre	$C4_{i1n}$	185.5/4	kN.s/m
Damping constant of lateral air suspension	$C5_{i11}$	3.336	kN.s/m
Height between c.o.g of carbody and lateral air suspension	Lz_1	0.735	m
Height between c.o.g of bogies and lateral air suspension	Lz_2	0.15	m
Height between c.o.g of bogies guide tyre	Lz_3	0.3	m
Height between guide and stabilising tyres	$Lz_4 + Lz_5$	1.085	m
Half length between right and left air suspension	Ly_2	1.415	m
Half length between right and left running tyre	Ly_4	0.2	m
Static feedback gain	K_{optm}	13000	N.s/m
Monorail vehicle speed	V	10	m/s

Appendix B

B.1 Equations of motion for monorail body

$$m_{11}\left(\ddot{z}_{11}-\left(V^2\left(\varphi_{\sec}-\theta_{x11}\right)/R_c\right)\right)=\sum_{i=1}^{2}\sum_{j=2}^{2}\sum_{n=!}^{2}\left\{-K1_{ijn}R1_{ijn}-C1_{ijn}\dot{R}1_{ijn}\right\}-f_{MR}$$

$$m_{11}\left(\ddot{y}_{11}-\left(V^2/R\right)+g\left(\varphi_{\sec}-\theta_{x11}\right)\right)=\sum_{i=1}^{1}\sum_{j=1}^{2}\sum_{n=1}^{2}\begin{Bmatrix}K5_{ijn}R5_{ijn}+C5_{ijn}\dot{R}5_{ijn}-K3_{ijn}R3_{ijn}-C3_{ijn}\dot{R}3_{ijn}\\-\left(K4_{ijn}R4_{ijn}+C4_{ijn}\dot{R}4_{ijn}\right)\delta_{1j}\end{Bmatrix}-f_{MR}$$

$$I_{x11}\ddot{\theta}_{x11}=\sum_{i=1}^{2}\sum_{j=1}^{1}\sum_{n=1}^{2}\left\{(-1)^n Ly_2\left(K1_{ijn}R1_{ijn}+C1_{ijn}\dot{R}1_{ijn}\right)-Lz_1\left(K5_{ijn}R5_{ijn}+C5_{ijn}\dot{R}5_{ijn}\right)\delta_{1j}+Lz_1 g\varphi_{\sec}\right\}$$
$$-Lz_1\left(fmr_{fm}+fmr_{rm}\right)+a\left(fmr_{fl}+fmr_{rl}\right)-b\left(fmr_{fr}+fmr_{rr}\right)$$

$$I_{y11}\ddot{\theta}_{y11}=\sum_{i=1}^{2}\sum_{j=1}^{1}\sum_{n=1}^{2}\left\{(-1)^i Lx_i\left(K1_{ijn}R1_{ijn}+C1_{ijn}\dot{R}1_{ijn}\right)\right\}-Lx_1\left(fmr_{fl}+fmr_{fr}\right)+Lx_2\left(fmr_{rl}+fmr_{rr}\right)$$

$$I_{z11}\ddot{\theta}_{z11}=\sum_{i=1}^{2}\sum_{j=1}^{1}\sum_{n=1}^{2}\left\{-(-1)^i Lx_i\left(K5_{ijn}R5_{ijn}+C5_{ijn}\dot{R}5_{ijn}\right)\right\}+Lx_1 fmr_{fm}-Lx_2 fmr_{rm}$$

(B1)

B.2 Equations of motion for front bogie

$$m_{21}\left(\ddot{z}_{21}-\left(V^2\left(\varphi_{\sec}-\theta_{x21}\right)/R\right)\right)=\sum_{i=1}^{1}\sum_{j=2}^{2}\sum_{n=1}^{2}\left\{\left(K1_{ijn}R1_{ijn}+C1_{ijn}\dot{R}1_{ijn}\right)\delta_{1j}-K2_{ijn}R2_{ijn}+C2_{ijn}\dot{R}2_{ijn}\right\}+fmr_{fr}+fmr_{fl}$$

$$m_{21}\left(\ddot{y}_{21}-\left(V^2/R\right)+g\left(\varphi_{\sec}-\theta_{x21}\right)\right)=\sum_{i=1}^{1}\sum_{j=1}^{2}\sum_{n=1}^{2}\begin{Bmatrix}K5_{ijn}R5_{ijn}+C5_{ijn}\dot{R}5_{ijn}-K3_{ijn}R3_{ijn}-C3_{ijn}\dot{R}3_{ijn}\\-\left(K4_{ijn}R4_{ijn}+C4_{ijn}\dot{R}4_{ijn}\right)\delta_{1j}\end{Bmatrix}+fmr_{fm}$$

$$I_{x21}\ddot{\theta}_{x21}=\sum_{i=1}^{1}\sum_{j=1}^{2}\sum_{n=1}^{2}\begin{Bmatrix}-(-1)^n Ly_2\left(K1_{ijn}R1_{ijn}+C1_{ijn}\dot{R}1_{ijn}\right)\delta_{1j}+(-1)^n Ly_4\left(K2_{ijn}R2_{ijn}+C2_{ijn}\dot{R}2_{ijn}\right)-Lz_2 g\varphi_{se_{fb}}\\-\left(Lz_3+Lz_4\right)\left(K3_{ijn}R3_{ijn}+C3_{ijn}\dot{R}3_{ijn}\right)-\left(Lz_3+Lz_4+Lz_5\right)\left(K4_{ijn}R4_{ijn}+C4_{ijn}\dot{R}4_{ijn}\right)\delta_{1j}\\-afmr_{fl}+bfmr_{fr}\end{Bmatrix}$$

$$I_{y21}\ddot{\theta}_{y21}=\sum_{i=1}^{1}\sum_{j=1}^{1}\sum_{n=1}^{2}\left\{(-1)^j Lx_3\left(K2_{ijn}R2_{ijn}+C2_{ijn}\dot{R}2_{ijn}\right)\right\}$$

$$I_{z21}\ddot{\theta}_{z21}=\sum_{i=1}^{1}\sum_{j=1}^{1}\sum_{n=1}^{2}\left\{-(-1)^j Lx_4\left(K3_{ijn}R3_{ijn}+C3_{ijn}\dot{R}3_{ijn}\right)\right\}$$

(B2)

B.3 Equations of motion for rear bogie

$$
\begin{aligned}
m_{22}\left(\ddot{z}_{22}-\left(V^2\left(\varphi_{\sec}-\theta_{x22}\right)/R\right)\right) &= \sum_{i=2}^{2}\sum_{j=2}^{2}\sum_{n=1}^{2}\left\{\left(K1_{ijn}R1_{ijn}+C1_{ijn}\dot{R}1_{ijn}\right)\delta_{1j}-K2_{ijn}R2_{ijn}+C2_{ijn}\dot{R}2_{ijn}\right\}+fmr_{rr}+fmr_{rl}\\
m_{22}\left(\ddot{y}_{21}-\left(V^2/R\right)+g\left(\varphi_{\sec}-\theta_{x22}\right)\right) &= \sum_{i=2}^{2}\sum_{j=1}^{2}\sum_{n=1}^{2}\left\{\begin{matrix}K5_{ijn}R5_{ijn}+C5_{ijn}\dot{R}5_{ijn}-K3_{ijn}R3_{ijn}-C3_{ijn}\dot{R}3_{ijn}\\-\left(K4_{ijn}R4_{ijn}+C4_{ijn}\dot{R}4_{ijn}\right)\delta_{1j}\end{matrix}\right\}+fmr_{rm}\\
I_{x22}\ddot{\theta}_{x22} &= \sum_{i=2}^{2}\sum_{j=1}^{2}\sum_{n=1}^{2}\left\{\begin{matrix}-(-1)^n Ly_2\left(K1_{ijn}R1_{ijn}+C1_{ijn}\dot{R}1_{ijn}\right)\delta_{1j}+(-1)^n Ly_4\left(K2_{ijn}R2_{ijn}+C2_{ijn}\dot{R}2_{ijn}\right)-Lz_2 g\varphi_{se_{rb}}\\-\left(Lz_3+Lz_4\right)\left(K3_{ijn}R3_{ijn}+C3_{ijn}\dot{R}3_{ijn}\right)-\left(Lz_3+Lz_4+Lz_5\right)\left(K4_{ijn}R4_{ijn}+C4_{ijn}\dot{R}4_{ijn}\right)\delta_{1j}\\-afmr_{rl}+bfmr_{rr}\end{matrix}\right\}\\
I_{y22}\ddot{\theta}_{y22} &= \sum_{i=2}^{2}\sum_{j=1}^{1}\sum_{n=1}^{2}\left\{(-1)^j Lx_3\left(K2_{ijn}R2_{ijn}+C2_{ijn}\dot{R}2_{ijn}\right)\right\}\\
I_{z22}\ddot{\theta}_{z22} &= \sum_{i=2}^{2}\sum_{j=1}^{1}\sum_{n=1}^{2}\left\{-(-1)^j Lx_4\left(K3_{ijn}R3_{ijn}+C3_{ijn}\dot{R}3_{ijn}\right)\right\}
\end{aligned}
\tag{B3}
$$

When (B1)–(B3) are rearranged in matrix form

$$\ddot{x}_s = M^{-1}C\dot{x}_s + M^{-1}Kx_s + M^{-1}Hf + M^{-1}LF_{dist} \tag{B4}$$

where M, C and K matrices represent the mass, damping and stiffness properties of the vehicle, respectively. H matrix stand for the location of the MR dampers. Guideway inputs are applied to the system by L vector. The state vector of the system is,

$$x_s = [z_{11}\quad y_{11}\quad \theta_{z11}\quad \theta_{y11}\quad \theta_{x11}\quad z_{21}\quad y_{21}\quad \theta_{z21}\quad \theta_{y21}\quad \theta_{x21}\quad z_{22}\quad y_{22}\quad \theta_{z22}\quad \theta_{y22}\quad \theta_{x22}]^T \tag{B5}$$

Each forces of the MR damper in f vector

$$f = \begin{bmatrix} Fmr_{fr} & Fmr_{fm} & Fmr_{fl} & Fmr_{rr} & Fmr_{rm} & Fmr_{rl} \end{bmatrix}^T \tag{B6}$$

Equation (B4) can be written as a state space equation as follows

$$
\begin{aligned}
\dot{x} &= Ax + Bu + WF_{dist}\\
&= \begin{bmatrix} 0_{6x6} & I_{6x6} \\ M^{-1}K & M^{-1}C \end{bmatrix} x + \begin{bmatrix} 0_{6x3} \\ M^{-1}H \end{bmatrix} f + \begin{bmatrix} 0_{6x2} \\ M^{-1}L \end{bmatrix} F_{dist}
\end{aligned}
\tag{B7}
$$

Estimation of the MR damper inner state z defined as

$$\dot{\hat{z}} = \dot{x}_{mr} - a_0 \left|\dot{x}_{mr}\right| \hat{z} \tag{B8}$$

The MR damper force should be replaced with its estimated value as follows

$$\hat{f} = \begin{bmatrix} \hat{z} & v\hat{z} & -\left|\dot{x}_{mr}\right|\hat{z} \end{bmatrix} \begin{bmatrix} \hat{\sigma}_a \\ \hat{\sigma}_0 \\ \widehat{\sigma_1 a_0} \end{bmatrix} + \begin{bmatrix} \dot{x}_{mr} & \dot{x}_{mr} v \end{bmatrix} \begin{bmatrix} \widehat{\sigma_1 + \sigma_2} \\ \hat{\sigma}_b \end{bmatrix} \tag{B9}$$

Estimation force equation of the MR damper can be defined as

$$\hat{f} = \hat{\theta}_{11}\hat{z} - \hat{\theta}_{13}\left|\dot{x}_{mr}\right|\hat{z} + \hat{\theta}_{21}\dot{x}_{mr} + \left(\hat{\theta}_{12}\hat{z} + \hat{\theta}_{22}\dot{x}_{mr}\right)v \tag{B10}$$